

Quantitative Comparison of Three- and Two-Dimensional PET with Human Brain Studies

Vesna Sossi, Terrence R. Oakes, Grace L.-Y. Chan, Michael Schulzer and Thomas J. Ruth
University of British Columbia/TRIUMF, Vancouver, British Columbia, Canada

The aim of this study was to test the quantitation accuracy of three-dimensional PET in brain scanning. **Methods:** Three-dimensional data from 11 human subjects were tested using ^{11}C -dihydrotetrabenazine, ^{11}C -Schering 23390 and ^{18}F -FDG as tracers. Two-dimensional scans were performed on the same subjects and the distribution volume, distribution volume ratio and local metabolic rate of glucose (LMRGlu) values obtained from these were used as reference. Three-dimensional data were processed as follows: iterative convolution subtraction scatter correction, detector normalization including radial and axial geometric factors, attenuation correction extracted from a two-dimensional transmission scan, Kinahan-Rogers reconstruction and region-of-interest-based sensitivity calibration. **Results:** No major systematic differences between the two methods were found. The agreement between the two-dimensional and three-dimensional data was within 5%. Although statistical analysis generally did not show this difference to be significant, reliability analysis indicated that comparing two-dimensional and three-dimensional data might introduce some inaccuracies. **Conclusion:** Three-dimensional PET yields quantitatively valid results for brain scanning.

Key Words: PET; two-dimensional PET; three-dimensional PET; quantitation

J Nucl Med 1998; 39:1714-1719

Septa-less or three-dimensional acquisition mode in PET has led to an approximately sixfold increase in tomograph sensitivity compared to the traditional two-dimensional acquisition mode and an approximately fourfold gain in the noise equivalent counting rate (NECR) (1) at radiotracer concentrations typically encountered in receptor and brain fluorodeoxyglucose (FDG) scanning. Such a performance gain in the NECR, which is proportional to the signal-to-noise ratio, is of extreme importance when the tracer kinetics of interest extend over several tracer half-lives. The increased statistical content of the data due to the increased NECR rate is also very important when performing neuroligand intervention studies, where changes in the tracer uptake are often relatively small and thus require good signal definition.

In spite of this significant gain in signal-to-noise ratio performance, the routine use of three-dimensional acquisition in brain receptor studies has been hindered by large dataset sizes, long reconstruction times and lack of quantitation, which is required for any kind of quantitative analysis. The lack of quantitation arises primarily from three causes, which are all related to the septa-less nature of three-dimensional PET: increased detection of scattered events (scatter) and random events (randoms) and the availability of many more lines of response (LORs) compared to two-dimensional acquisition. This article specifically addresses the quantitation issue, and it does not try to quantify the benefits of the statistical superiority of three-dimensional PET compared to the slice-acquisition

mode, which has been addressed already by other authors (2,3). The quantitation accuracy of an acquisition mode is heavily dependent on the algorithms that are used to produce the images, since it is possible that the quantitation accuracy may vary as a function of algorithms used to produce the images. Therefore, an assessment of quantitation accuracy of three-dimensional PET inherently presents a test and evaluation of the algorithms used in the imaging process. The work presented here is based on a previously developed three-dimensional data processing protocol using phantom studies. Data processed with this protocol yielded an image quantitation quality that was comparable to that obtained from data acquired in two-dimensional mode (4,5). The protocol involves an iterative convolution subtraction scatter correction algorithm with spatially invariant scatter kernel (6), a detector normalization that includes radial and axial geometric factors and accounts for individual detector efficiency variations (7,8), attenuation correction extracted from a two-dimensional transmission scan, a three-dimensional filtered backprojection reconstruction algorithm (9) and a region-of-interest-based sensitivity calibration (5), applied in this order.

This work tests the performance of the same protocol with human studies, a more challenging environment, since human studies present a wider variety of scanning conditions compared to phantom studies. Since the real radiotracer distribution is not known when human subjects are studied, three-dimensional and two-dimensional scans of the same patients were performed and the results from the two-dimensional studies were used as reference in the evaluation of the performance of the three-dimensional protocol. Eleven human subjects were used, using ^{11}C -dihydrotetrabenazine (DTBZ), ^{11}C -Schering 23390 (Sch) and ^{18}F -FDG as tracers. DTBZ and Sch are used to study the integrity of striatal presynaptic and postsynaptic monoaminergic terminals respectively, while FDG is characterized by a more global distribution in the brain. The following analysis figures of merit were used for the neuroreceptor studies: striatum-to-occipital cortex ratio, striatum-to-cerebellum ratio, distribution volume (DV) (10), and distribution volume ratio (DVR) (11) with occipital cortex and cerebellar input function. For the FDG studies LMRGlu (12) analysis was performed. The comparison showed a good quantitative agreement between the two acquisition modes. However, reliability analysis results indicate that a direct comparison between data acquired in two-dimensional and three-dimensional modes might still introduce some bias. In this study, two-dimensional and three-dimensional will be used loosely to indicate results obtained from data acquired in two-dimensional and three-dimensional mode, respectively.

MATERIALS AND METHODS

All scans were performed on a Siemens/CTI ECAT 953B (CTI, Knoxville, TN) (13), that has 31 imaging planes, an in-plane resolution of 5.6 mm, a slice width of 4.0 mm in two-dimensional mode and axial resolution in three-dimensional mode of 6 mm.

Received Aug. 20, 1997; revision accepted Jan. 23, 1998.
For correspondence or reprints contact: Vesna Sossi, PhD, 4004 Wesbrook Mall, Vancouver, B.C. V6T 2A3, Canada.

Algorithms

The processing protocol described later was found to be optimum using phantom studies (4,5), which were used to test the scatter, normalization and calibration corrections and the order in which they should be applied. Dead time, randoms and attenuation correction were deemed to be adequate for the acquisition conditions encountered in brain receptor and FDG imaging, which do not stress the counting rate capabilities of the scanner.

Scatter Correction. The scatter correction used in this protocol is an iterative convolution subtraction method developed by Bailey et al. (6). The scatter kernel is a product of a monoexponential function and a constant scatter fraction. The coefficient of the exponent was experimentally determined to be -0.1 and the scatter fraction to be 0.31 .

Detector Normalization. The detector normalization correction includes two components, one that corrects for the efficiency variation due to the scanner geometry and one that corrects for the efficiency variations due to electronic drift. The geometric correction includes radial and axial geometric factors that account for the efficiency variation within a detector ring and between different detector rings. Individual detector efficiency factors are calculated from a three-dimensional fan of LORs after the geometric efficiency difference was factored out of the data. The geometric and the individual detector efficiencies were derived from separate high statistics scans of a uniform plane source (4,5,7) and were used to correct the acquired data on an LOR after scatter correction. The normalization correction was applied after scatter correction since phantom studies demonstrated this to be the optimal correction application order (4,5).

Attenuation Correction. The attenuation correction was obtained by forward projecting an attenuation image obtained from a two-dimensional transmission scan and blank scan.

Sensitivity Calibration and Image Reconstruction. The sensitivity calibration factors were obtained from scatter-, normalization- and attenuation-corrected reconstructed data of an elliptical phantom ($14.5 \times 19 \times 19.4 \text{ cm}^3$) (3) scan. An ROI encompassing most of the phantom image was placed on each image plane and the conversion factors between the region of interest (ROI) average count/voxel value and the independently measured concentration value ($\mu\text{Ci/ml}$), using a calibrated well counter, were calculated for each image plane (5). The sensitivity calibration factors were applied to the images after they had been reconstructed using the Kinahan-Rogers reconstruction algorithm using a Hann filter with $0.4/\text{bin}$ cutoff frequency for the neuroligand studies and $0.5/\text{bin}$ cutoff frequency for the FDG studies.

The two-dimensional data were processed using the standard CTI ECAT software (13) that includes LOR-based detector normalization, convolution subtraction type scatter correction, attenuation correction obtained from the ratio of a transmission and blank scan, filtered backprojection reconstruction and calibration factors obtained as described previously. Images were reconstructed using a Hann filter to the same resolution as the images obtained from the three-dimensional data to minimize sources of difference in the results of the two-dimensional–three-dimensional comparison.

Study Selection

Two different kinds of tracer were selected for this validation study because of their different temporal and spatial distribution properties and different spatial location of biologically interesting ROIs. When the ^{11}C -labeled dopaminergic ligands DTBZ and Sch are used, the ROIs are typically the striata, occipital cortex and cerebellum. These studies generally are characterized by a greatly varying number of counts in each acquired time frame (1 *M* counts/frame to 24 *M* counts/frame) due to a varying duration of

the scanning interval and rapid tracer decay, thus requiring algorithm stability over a wide range of data statistical content. The ^{18}F -labeled FDG studies are generally static scans, with the number of events only proportional to the injected dose and scan duration. The ROIs are more widely spread within the brain volume, thus requiring the quantitation accuracy to be highly spatially uniform.

Tracer Preparation. Carbon-11-Sch was synthesized by *N*-methylation of the desmethyl precursor analogs Schering 24518 using [^{11}C]methyl iodide (12). The desmethyl precursor of Sch was supplied by Schering Plow Corporation, Bloomfield, NJ. The specific activity was 1988 ± 568 (mean \pm std) Ci/mmol at ligand injection, and the radiochemical purity was $>99\%$.

Carbon-11-(\pm)- α -dihydrotrabenazine was prepared by a modification of the method described by Kilbourn et al. (15). Briefly, (\pm)-9-O-desmethyl- α -dihydrotrabenazine was methylated with ^{11}C -methyl iodide in a mixture of dimethyl sulfoxide/NaOH. The product was purified by high-performance liquid chromatography and obtained with $>95\%$ radiochemical purity and a specific activity of $2\text{--}3 \text{ Ci}/\mu\text{mol}$ at end of bombardment. The specific activity was 1294 ± 278 (mean \pm std) Ci/mmol at ligand injection. Fluorine-18-FDG was synthesized by the electrophilic method using ^{18}F -acetyl hypofluorite.

Three-Patient Protocol

Neuroligand Studies. For each of the studies, a two-dimensional and a three-dimensional scan with 16 time frames each ($4 \times 60 \text{ sec}$, $3 \times 120 \text{ sec}$, $8 \times 300 \text{ sec}$, $1 \times 600 \text{ sec}$) were acquired in alternate order (two-dimensional followed by three-dimensional and reversed) on four normal volunteer subjects (26–50 yr of age) using DTBZ and four different subjects (34–76 yr of age) using Sch as tracers. In each subject, the injected radioactivity was 7 mCi. Twenty-three plasma blood samples were collected during the duration of the scan, five of which were analyzed for metabolites (16,17). A windowed transmission scan was performed on each subject before tracer injection for the three-dimensional studies, while a nonwindowed transmission scan, consistent with our traditional two-dimensional protocol, was used for the two-dimensional studies.

FDG Studies. A 20-min two-dimensional FDG scan starting 40 min after injection was performed followed immediately by a 20-min three-dimensional scan on three subjects (29–36 yr of age). The injected radiotracer dose was 2 mCi. Twenty-eight plasma samples were collected during the scans. A postinjection transmission scan was performed on these subjects immediately before emission data collection and used to correct both the two-dimensional and three-dimensional studies.

All subjects gave written informed consent before each scan. The study was approved by the UBC Human Ethics Committee.

Data Analysis

Neuroligand Studies. The dopaminergic ligand studies were analyzed in five different ways by calculating the following analysis figures of merit (AFOM): striatum/occipital cortex ratio (S/OC), striatum/cerebellum ratio (S/Cer), total D, that requires a blood input function, and DVRs with input function derived from the occipital cortex (DVR_{oc}) and from the cerebellum (DVR_{cer}). The ratios S/OC and S/Cer were calculated on the data summed over the last 30 min of the study and no additional model was applied to the data. By using the OC (Cer) values as denominators, data from the same (different) image plane are used, causing the method to be less (more) sensitive to axial nonuniformity differences between two-dimensional and three-dimensional studies. The same observation regarding the sensitivity to the axial distribution of the data holds for the situations where the occipital cortex or the cerebellar input functions are used. In the calculation of the Sch DVR_{cer} , a k_2 value of $0.10099/\text{min}$ was used, while a k_2 of

0.061326/min was used for the Sch DVR_{oc}. No term including the k2 value was considered in the DTBZ DVR calculation due to the fast equilibration of this tracer. When the blood input function is used, where the plasma tracer concentration is measured by a calibrated well counter, the tomograph absolute calibration is tested in addition to the other aspects of the quantitation algorithms.

FDG Studies. A local glucose metabolic rate analysis was performed on the images obtained from the FDG scans. This analysis requires an independently measured plasma tracer concentration as input function. The following values were used for the rate constants: 0.1020 mg/min/(100 gr of tissue) (k1), 0.1300 mg/min/(100 gr of tissue) (k2), 0.0620 mg/min/(100 gr of tissue) (k3), 0.0068 mg/min/(100 gr of tissue) (k4) and the value of the lumped constant was 0.420.

Region of Interest Placement, Neuroligand Studies. For each subject, one ROI was placed on each caudate, three on each putamen, six on the occipital cortex on five adjacent image planes and two larger ROIs on two different adjacent image planes on the cerebellar region.

Region of Interest Placement, FDG Studies. For the FDG studies, the LMRGlu were calculated for 64 ROIs, with a radius of 7.5 mm each, which were placed on the frontal cortex, thalamus, striata, occipital cortex and cerebellum covering a slice range from Slice 3 to Slice 29 inclusive.

Figures of Merit

Neuroligand Studies. The fractional difference between the AFOM obtained from three-dimensional data and two-dimensional data [(two-dimensional-three-dimensional)/(0.5*(three-dimensional + two-dimensional))] averaged over subjects was considered as a figure of merit when comparing the two acquisition modes.

In addition, the following statistical analysis (18) was performed on the data to quantify the significance of the difference (two-dimensional-three-dimensional). First, a crossover analysis using a two-sided paired Student's t-test was performed to check for period effect and for two-dimensional versus three-dimensional or treatment effect. Second, calculation of reliability coefficients (19) from an ANOVA analysis of the components of variance. Reliability is defined as $SDB(2)/(STDB(2)+STDW(2))$, where STDB is the standard deviation between subjects and STDW is the standard deviation within repeated measurements in the same subject. Here results of the two-dimensional and three-dimensional data from the same subject were considered as repeated measurements, that is, the reproducibility between results obtained from the two-dimensional and three-dimensional data was compared to the variance of the results between different subjects. Third, a plot of two-dimensional-three-dimensional results versus two-dimensional + three-dimensional results was performed for each AFOM

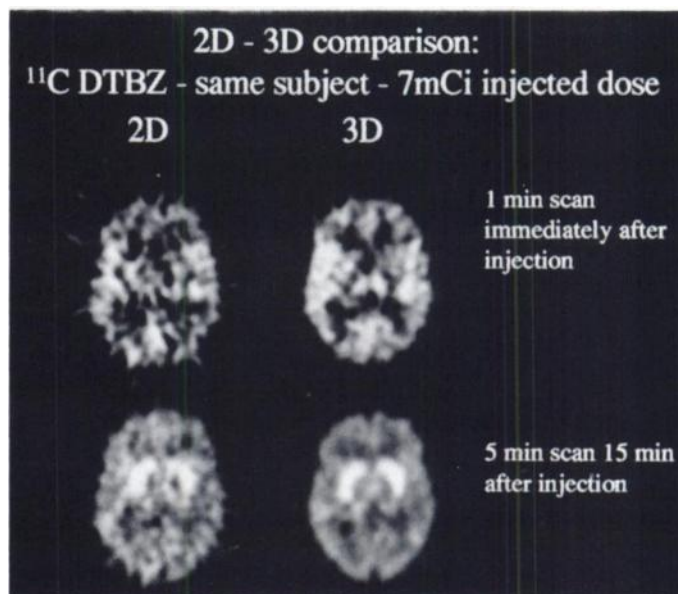


FIGURE 1. Comparison of two-dimensional and three-dimensional DTBZ studies. Top left and right images show 1-min frames acquired 1 min after injection for two-dimensional and three-dimensional acquisition modes, respectively. Bottom images show same comparison for 5-min frames acquired 15 min after injection.

to check if the magnitude of the difference is a function of the value of the AFOM.

FDG Studies. In the FDG studies, the variation between the LMRGlu obtained from the three-dimensional and two-dimensional data was similarly expressed in terms of fractional difference for each ROI and the mean and standard deviation of the difference over all ROIs and over groups of anatomically meaningful ROIs was calculated. In this study, results were expressed for each patient separately and no additional statistical analysis was performed on these data.

RESULTS

Neuroligand Studies

Figure 1 shows the large improvement in image quality when the three-dimensional acquisition mode is used compared to the two-dimensional mode. Two selected frames are shown: a 1-min frame acquired 1 min after injection and a 5-min frame acquired 15 min after injection. The noise in the three-dimensional images is reduced noticeably compared to the two-dimensional images.

Fractional Difference. Results for the fractional difference comparison of the S/OC, S/Cer ratios and DV, DVR_{oc} and

TABLE 1
Results for the Fractional Difference Comparison of the S/OC, S/Cer Ratios and DV, DVR_{oc} and DVR_{cer}*

Analysis figure of merit	Sch tracer			DTBZ tracer		
	Caudate ROI	Putamen ROI	OCC cortex ROI	Caudate ROI	Putamen ROI	OCC cortex ROI
S/OC	-0.03 ± 0.04	-0.05 ± 0.05	—	-0.03 ± 0.06	-0.03 ± 0.07	—
S/Cer	-0.05 ± 0.04	-0.08 ± 0.05	—	-0.07 ± 0.08	-0.07 ± 0.08	—
DV	-0.05 ± 0.13	-0.09 ± 0.12	0.00 ± 0.13	-0.02 ± 0.11	-0.05 ± 0.06	0.00 ± 0.05
DVR _{oc}	-0.07 ± 0.04	-0.10 ± 0.05	—	-0.03 ± 0.05	-0.03 ± 0.05	—
DVR _{cer}	-0.09 ± 0.04	-0.11 ± 0.07	-0.03 ± 0.03	-0.07 ± 0.05	-0.07 ± 0.06	-0.04 ± 0.03

((2D - 3D)/(0.5(3D + 2D))) of S/OC, S/Cer, DV, DVR_{oc} and DVR_{cer} averaged over 4 subjects for the Sch and DTBZ studies.

S/OC = striatum/occipital cortex ratio; S/Cer = striatum/cerebellum ratio; DV = distribution volume; DVR_{oc} = distribution volume ratio_{occipital}; DVR_{cer} = distribution volume ratio_{cerebellum}; Sch = ¹¹C-schering 23390; DTBZ = ¹¹C-dihydrotrabenzazine; OCC = occipital; ROI = region of interest.

TABLE 2

T and P Values for Treatment Effect (Two-Dimensional versus Three-Dimensional) for the Two Tracers as Found by Crossover Analysis ($p < 0.05$)

Analysis figure of merit	Sch tracer						DTBZ tracer					
	Caudate		Putamen		OCC cortex		Caudate		Putamen		OCC cortex	
	T	P	T	P	T	P	T	P	T	P	T	P
S/OC	-1.20	0.35	-3.97	0.06	—	—	-1.39	0.30	-1.02	0.42	—	—
S/Cer	-2.35	0.14	-5.41	0.033	—	—	-1.73	0.23	-1.68	0.24	—	—
DV	-1.71	0.23	-2.65	0.12	-0.20	0.86	-0.36	0.75	-3.34	0.08	-0.01	0.99
DVR _{oc}	-2.97	0.10	-7.92	0.016	—	—	-1.52	0.27	-2.01	0.18	—	—
DVR _{cer}	-4.34	0.049	-4.22	0.052	-2.22	0.16	-2.18	0.16	-2.65	0.12	-3.31	0.08

Sch = ¹¹C-Schering 23390; DTBZ = ¹¹C-dihydrotrabenazine; OCC = occipital; S/OC = striatum/occipital cortex ratio; S/Cer = striatum/cerebellum ratio; DV = distribution volume; DVR_{oc} = distribution volume ratio_{occipital}; DVR_{cer} = distribution volume ratio_{cerebellum}.

DVR_{cer} are presented in Table 1, separately for the caudate, putamen and, where applicable, occipital cortex, ROIs for the data obtained from the Sch and DTBZ tracers. This difference has a component due to scan-rescan variability and a component due to potential differences between two-dimensional and three-dimensional data quantitation. Similar results were obtained with the two tracers. The data showed a trend for the three-dimensional to give higher values for all AFOM where the striatal ROIs are involved. There was no difference in the two-dimensional–three-dimensional comparison between the caudate and putamen ROIs indicating that comparable image uniformity in the region of the striatal image was achieved with both acquisition modalities in contrast to previous studies (20). There was no significant difference in fractional difference when DV and DVR_{cer} were calculated for the occipital cortex region indicating similar axial image uniformity between two-dimensional and three-dimensional modes. This was confirmed by the fact that the fractional difference is the same for S/OC and S/Cer as well as for DVR_{oc} and DVR_{cer}, which use the occipital cortex and cerebellum as reference regions, respectively.

Statistical Analysis. Results of the crossover design analysis are shown in Table 2. Data from the left and right striatum were averaged since no significant difference between the two sides was observed. Time-period effect reached significance only for the DV calculated for the caudate ROIs ($p = 0.045$) when Sch was used as a tracer, indicating that there might be a morning-afternoon effect. Detailed investigation of this effect was beyond the scope of this study. The treatment (two-dimensional versus three-dimensional) effect yielded the following results for Sch: marginally significant difference between the two-dimensional and three-dimensional was found for the DVR_{cer} for the caudate ($p = 0.049$) and putamen ($p = 0.052$). For the DVR_{oc} and for the S/Cer, a significant difference between the two-dimensional and three-dimensional modes was found for the putamen ($p = 0.016$ and $p = 0.033$, respectively), while no significant difference was found for the DV and S/OC. No significant difference was found when DTBZ was used as the tracer. Results of the reliability coefficient analysis are presented in Table 3 for both tracers. The slope analysis showed that the magnitude of the AFOM did not affect the magnitude of the difference between two-dimensional and three-dimensional modes, as expected.

FDG Studies

The fractional difference of the LMRGlu values averaged overall ROIs between data obtained from the three-dimensional mode and data obtained from the two-dimensional studies was -0.01 ± 0.08 for the first patient, -0.10 ± 0.06 for the second

patient and -0.03 ± 0.10 for the third patient. The difference did not depend on the ROI location as presented in Table 4, where the fractional difference is expressed for each set of anatomically significant ROIs.

DISCUSSION

The results of the fractional difference between the values of the AFOM obtained from the neuroreceptor studies indicated that the three-dimensional processing protocol described earlier showed a tendency of yielding slightly higher values compared to results from data acquired in the two-dimensional mode. The trend was not found to be significant after applying statistical analysis except in a few isolated cases. A close, but not perfect, match also was detected by reliability analysis. It is interesting to observe the apparent discrepancy in the reliability results. The reliability of the AFOM for Sch was much lower than that obtained from the DTBZ data, except for DV, where it was approximately 0.9. To correctly interpret this result, it is necessary to know the reliability characteristic of the tracer when the same acquisition modality is being used (intrinsic reliability). Sch exhibited a high intrinsic reliability for all AFOM (around 0.9), except for DV (around 0.5), which indicated poor within-subject reproducibility for this particular AFOM (16). Since the intrinsic within-subject reproducibility

TABLE 3
Reliability Coefficients for Analysis Figure of Merit for Each Set of ROI, Sch and DTBZ Data

Analysis figure of merit	ROI	Reliability	
		Sch	DTBZ
S/OC	Caudate	0.50	0.73
	Putamen	0.51	0.79
S/Cer	Caudate	0.60	0.50
	Putamen	0.60	0.59
DV	Caudate	0.91	0.45
	Putamen	0.89	0.83
DVR _{oc}	OC	0.91	0.45
	Caudate	0.25	0.73
DVR _{cer}	Putamen	0.0	0.88
	Caudate	0.35	0.51
	Putamen	0.09	0.68
	OC	0.44	0.55

ROI = region of interest; Sch = ¹¹C-Schering 23390; DTBZ = ¹¹C-dihydrotrabenazine; S/OC = striatum/occipital cortex ratio; S/Cer = striatum/cerebellum ratio; DV = distribution volume; DVR_{oc} = distribution volume ratio_{occipital}; DVR_{cer} = distribution volume ratio_{cerebellum}; OC = occipital cortex.

TABLE 4
 Fractional Difference $(2D - 3D)/(0.5*(2D+3D))$ for the FDG Data for Each of the Anatomically Defined Regions of Interest

	Subject 1		Subject 2		Subject 3	
ROI region	Fract difference	Std	Fract difference	Std	Fract difference	Std
Frontal cortex	0.01	0.05	0.07	0.05	0.05	0.04
Striatum	0.01	0.06	0.11	0.05	0.03	0.07
Occipital cortex	0.01	0.10	0.10	0.07	0.00	0.11
Thalamus	0.05	0.08	0.10	0.03	0.04	0.11
Cerebellum	-0.02	0.11	0.13	0.09	0.12	0.08

*Std is the standard deviation of the fractional difference over regions of interest (ROIs) placed on the same anatomical ROI.

was poor for DV, the impact introduced by the varying acquisition mode would be minimal, which resulted in the high reliability values in this study (Table 3). The same considerations held for the reliability obtained from the DTBZ data. In other studies, we found that the intrinsic reliability for DTBZ was, in fact, lower than that obtained when Sch was used as the tracer, thus, again minimizing the effect of the acquisition mode, which resulted in the higher reliability values in Table 3. Although the reliability values indicated that it is not advisable to directly compare data obtained from the two acquisition modalities, they still showed that the results obtained from the two-dimensional and the three-dimensional modes were in good agreement, improving previously published results (2,20,21).

The two-dimensional–three-dimensional comparison was performed using several analysis methods. Although there might be some debate about which of these methods is the most biologically significant for each tracer, all were used in this validation study, since each of them explores a different aspect of the data. Results were consistent for all analysis methods, which indicated that there are no noticeable local differences between the data acquired in two-dimensional and three-dimensional modes.

In the case of the FDG data, two-dimensional results yielded systematically slightly higher LMRGlu compared to the three-dimensional data. The difference appeared to be an overall offset as opposed to regional differences. This difference might be due to the fact that a windowed transmission scan was used to calculate the attenuation correction factors for the two-dimensional scan, while the tomograph sensitivity in two-dimensional mode was calibrated using a nonwindowed transmission scan for consistency with our early two-dimensional scans, performed when rod windowing software was not available yet. However, the absence of regional differences indicated that there were no significant uniformity differences between the two acquisition modes.

CONCLUSION

Three-dimensional PET yielded an approximately fourfold gain in the noise equivalent counting rate (I) at radiotracer concentrations typically encountered in receptor and brain FDG studies, thus significantly improving the statistical image quality and/or allowing for longer studies. In the present study, the quantitative aspect of three-dimensional PET in brain studies has been evaluated since quantitation is often a strong requirement in image analysis. Biologically meaningful results obtained from three-dimensional studies were compared to those obtained from two-dimensional studies performed on the same subjects. S/OC , S/Cer , DVR_{oc} , DVR_{cer} and DV were used as figures of merit for the neuroligand studies and LMRGlu was used for the FDG studies. Images from three-dimensional PET data were processed with the following protocol: iterative convolution subtraction scatter correction method, a detector

normalization with axial and radial geometric factors, attenuation correction, FBP reconstruction algorithm and ROI-based sensitivity calibration. The difference between the results obtained from the two-dimensional and three-dimensional PET data in neuroreceptor studies was generally around 5%, indicating no major systematic differences and good agreement between the two acquisition and processing modes. Statistical analysis performed on the results of the neuroreceptor studies on our population sample did not show this difference to be significant, except in a few isolated cases. Reliability analysis, however, indicated that comparing results directly from the two-dimensional and the three-dimensional acquisition modes might introduce some inaccuracies. Good agreement between the two-dimensional and three-dimensional data was confirmed also by the LMRGlu analysis applied to the FDG studies, where the ROIs sampled a large area of the brain. The imaging protocols and subsequent analysis methods tested in this study involved scanning conditions with a wide range of the number of acquired counts and different locations of ROIs in the brain image and, thus, provided a demanding test ground for the algorithms performance. Three-dimensional PET quantitation accuracy is adequate for brain studies, however, a direct comparison between two-dimensional and three-dimensional PET is not recommended when inaccuracies of the order of 5% cannot be neglected.

ACKNOWLEDGMENTS

The authors thank Dr. Jon Stoessl, E. Mak for the statistical analysis, the UBC/TRIUMF PET team for tracer production and, in particular, Carolyn English and Jessamyn Wudel for data acquisition, Teresa Dobko for the image analysis, Scott Morrison for software development and Dr. Peter Liddle and Carol Ln. for the FDG studies. This study was supported by a Canadian Medical Research Group Grant and a U.S. N.I.H. Fellowship F32-CA67486 funded by the U.S. National Cancer Institute.

REFERENCES

1. Strother SC, Casey ME, Hoffman EJ. Measuring PET scanner sensitivity: relating count rates to image signal-to-noise ratios using noise equivalent counts. *IEEE Trans of Nucl Med* 1990;37:2: 783–788.
2. Rakshi JS, Bailey DL, Morrish PK, Brooks DJ. Implementation of 3D acquisition, reconstruction and analysis of dynamic [^{18}F]fluorodopa studies. *Quantification of brain using PET*. San Diego: Academic Press; 1996:82–87.
3. Kohlmyer SG, Mankoff DA, Lewellen TK, Kaplan MS. Comparison of 2D and 3D qualitative whole-body PET without attenuation or scatter correction. In: Del Guerra A, ed. *Proceedings of the 1996 IEEE/MIC*. Piscataway, NJ: IEEE; 1996:1367–1371.
4. Sossi V, Oakes TR, Ruth TJ. Evaluation of the ICS and DEW scatter correction methods for low statistical content scans. In: Del Guerra A, ed. *Proceedings of the 1996 IEEE/MIC*. Piscataway, NJ: IEEE; 1996:1537–1541.
5. Sossi V, Oakes TR, Ruth TJ. A phantom study evaluating the quantitative aspect of 3D PET imaging of the brain. *Phys Med Biol*, 1998 in press.
6. Bailey DL, Meikle S. A convolution subtraction scatter correction method for 3D PET. *Phys Med Biol* 1994;39:411–424.
7. Stazyk MW, Sossi V, Buckley KR, Ruth TJ. Normalization measurement in septa-less PET scanners[Abstract]. *J Nucl Med* 1994;35:5: 41P.
8. Oakes TR, Sossi V, Ruth TJ. Normalization for 3D PET with a low-scatter planar source and measured geometric factors. *Phys Med Biol* 1998;43:961–972.

9. Kinahan PE, Rogers JG. Analytic 3D image reconstruction using all detected events. *IEEE TNS* 1989;36:964-968.
10. Logan J, Fowler JS, Volkow ND, et al. Graphical Analysis of reversible radioligand binding from time-activity measurements applied to [^{11}C -methyl(-)-cocaine PET studies in human subjects. *J Cereb Blood Flow Metab* 1990;10:740-747.
11. Logan J, Fowler JS, Volkow ND, Wang G-J, Ding Y-S, Alexoff DL. Distribution volume ratios without blood sampling from graphical analysis of PET data. *JCBF* 1996;16:834-840.
12. Phelps ME, Huang SC, Hoffman EJ, Selinns C, Sokoloff L, Kuhl DE. Tomographic measurement of local cerebral glucose metabolic rate in humans with ^{18}F -2-fluoro-2-deoxy-D-glucose: validation of method. *Ann Neurol* 1979;6:371-388.
13. Spinks TJ, Jones T, Bailey DJ, et al. Physical performance of a positron tomograph for brain imaging with retractable septa. *Phys Med Biol* 1992;37:8: 1637-1655.
14. Ravert HT, Wilson AA, Dannals RF, Wong DF, Wagner HN. Radiosynthesis of a selective dopamine D-1 receptor antagonist: R(+)-7-chloro-8-hydroxy-3-[^{11}C]methyl-1-phenyl-1,2,3,4,5-tetrahydro-1H-3-benzazepine ([^{11}C]SCH 23390). *Appl Radiat Isot* 1987;38:305-306.
15. Kilbourn, Lee L, Vander Borgh T, Jewett D, Frey K. Binding of α -dihydrotrabenzazine to the vesicular monoamine transporter is stereospecific. *Eur J Pharmacol* 1995;278:249-252.
16. Chan GL-Y, Holden JE, Stoessl J et al. Reproducibility of [^{11}C]SCH 23390 PET in normal human subjects. *J Nucl Med* 1998;39:792-797.
17. Frey KA, Koeppel RA, Kilbourn MR. Presynaptic monoaminergic vesicles in Parkinson's disease and normal aging. *Ann Neurol* 1996;40:873-884.
18. Fleiss JL. *The design and analysis of clinical experiment*. New York: John Wiley & Sons: 1986:263-290.
19. Scheffe H. *The analysis of variance*. New York: John Wiley & Sons; 1959:221-260.
20. Trebossen R, Bendriem B, Fontaine A et al. Quantitation of the [^{18}F]fluorodopa uptake in the human striata in 3D PET with the ETM scatter correction. *Quantification of brain using PET*. San Diego: Academic Press; 1996:88-92.
21. Townsend DW, Price JC, Lopresti BJ et al. Scatter correction for brain receptor quantitation in 3D PET. *Quantification of brain using PET*. Academic Press; 1996:76-81.

Significance of Nonuniform Attenuation Correction in Quantitative Brain SPECT Imaging

Nallakkandi Rajeevan, I. George Zubal, S. Quinn Ramsby, Sami S. Zoghbi, John Seibyl and Robert B. Innis

Departments of Diagnostic Radiology and Psychiatry, Yale University School of Medicine, New Haven; and Veterans Affairs Connecticut, New Haven, Connecticut

The purposes of this study were to develop a method for nonuniform attenuation correction of ^{123}I emission brain images based on transmission imaging with a longer-lived isotope (i.e., ^{57}Co) and to evaluate the relative improvement in quantitative SPECT images achieved with nonuniform attenuation correction. **Methods:** Emission and transmission SPECT scans were acquired on three different sets of studies: a heterogeneous brain phantom filled with ^{123}I to simulate the distribution of dopamine transporters labeled with 2 β -carbomethoxy-3 β -(4- ^{123}I -iodophenyl)tropane (^{123}I - β -CIT); nine healthy human control subjects who underwent transmission scanning using two separate line sources (^{57}Co and ^{123}I); and a set of eight patients with Parkinson's disease and five healthy control subjects who received both emission and transmission scans after injection of ^{123}I - β -CIT. Attenuation maps were reconstructed using a Bayesian transmission reconstruction algorithm, and attenuation correction was performed using Chang's postprocessing method. The spatial distribution of errors within the brain was obtained from attenuation correction factors computed from uniform and nonuniform attenuation maps and was visualized on a pixel-by-pixel basis as an error image. **Results:** For the heterogeneous brain phantom, the uniform attenuation correction had errors of 2%-6.5% for regions corresponding to striatum and background, whereas nonuniform attenuation correction was within 1%. Analysis of ^{123}I transmission images of the nine healthy human control subjects showed differences between uniform and nonuniform attenuation correction to be in the range of 6.4%-16.0% for brain regions of interest (ROIs). The human control subjects who received transmission scans only were used to generate a curvilinear function to convert ^{57}Co attenuation values into those for ^{123}I , based on a pixel-by-pixel comparison of two coregistered transmission images for each subject. These values were applied to the group of patients and healthy control subjects who received transmission ^{57}Co scans and emission ^{123}I scans after injection of ^{123}I - β -CIT. In comparison to nonuniform attenuation correction as the gold standard, uniform attenuation with the ellipse drawn around the transmission image caused an ~5% error, whereas placement of the ellipse around the emission image caused a 15% error. **Conclusion:** Nonuniform

attenuation correction allowed a moderate improvement in the measurement of absolute activity in individual brain ROIs. When images were analyzed as target-to-background activity ratios, as is commonly performed with ^{123}I - β -CIT, these outcome measures showed only small differences when Parkinson's disease patients and healthy control subjects were compared using nonuniform, uniform or even no attenuation correction.

Key Words: quantitative SPECT; nonuniform attenuation correction; brain imaging

J Nucl Med 1998; 39:1719-1726

The importance of nonuniform attenuation correction in SPECT imaging of highly heterogeneous sections of the body, like the thorax, is well recognized (1). However, its significance in quantitative brain SPECT imaging has not been so well documented. Routine clinical brain SPECT imaging still uses uniform attenuation correction, assuming that the head has homogeneous attenuation properties and elliptical cross-sections. Here, we examine the heterogeneity of the head and analyze the significance of nonuniform attenuation correction in quantifying radioligand distribution in the brain using SPECT imaging.

Various methods for attenuation correction in SPECT have been proposed. These methods can be classified as:

1. Object space postprocessing methods (2);
2. Attenuation-weighted backprojection (3,4); and
3. Iterative projection-backprojection methods (5-8).

In postprocessing methods, such as Chang's algorithm (2), an attenuation correction factor for each voxel in the object is first computed from a map of the attenuation coefficients of the object. These correction factors are then applied to the reconstructed emission image. In the attenuation-weighted backprojection methods, the image reconstruction filter (i.e., ramp filter multiplied by a window function) is modified in such a way that the filter is a function of the constant attenuation coefficient for the object. In iterative methods, pseudoprojections of an estimated emission image through the attenuation

Received Oct. 1, 1997; revision accepted Jan. 14, 1998.

For correspondence or reprints contact: N. Rajeevan, PhD, Yale University and VA Connecticut/116A2, 950 Campbell Avenue, West Haven, CT 06516.